HHS Public Access

Author manuscript

J Neural Eng. Author manuscript; available in PMC 2017 August 03.

Published in final edited form as:

J Neural Eng. 2015 April ; 12(2): 026003. doi:10.1088/1741-2560/12/2/026003.

Rapid evaluation of the durability of cortical neural implants using accelerated aging with reactive oxygen species

Pavel Takmakov[1], **Kiersten Ruda**[2], **K Scott Phillips**[1], **Irada S Isayeva**[1], **Victor Krauthamer**[2], and **Cristin G Welle**[2]

[1]Division of Biology, Chemistry and Material Science, Office of Science and Engineering Laboratories, Center for Devices and Radiological Health, US Food and Drug Administration, White Oak Federal Research Center, Silver Spring, MD, USA

[2]Division of Biomedical Physics, Office of Science and Engineering Laboratories, Center for Devices and Radiological Health, US Food and Drug Administration, White Oak Federal Research Center, Silver Spring, MD, USA

Abstract

Objective—A challenge for implementing high bandwidth cortical brain–machine interface devices in patients is the limited functional lifespan of implanted recording electrodes. Development of implant technology currently requires extensive non-clinical testing to demonstrate device performance. However, testing the durability of the implants *in vivo* is time-consuming and expensive. Validated *in vitro* methodologies may reduce the need for extensive testing in animal models.

Approach—Here we describe an *in vitro* platform for rapid evaluation of implant stability. We designed a reactive accelerated aging (RAA) protocol that employs elevated temperature and reactive oxygen species (ROS) to create a harsh aging environment. Commercially available microelectrode arrays (MEAs) were placed in a solution of hydrogen peroxide at 87 °C for a period of 7 days. We monitored changes to the implants with scanning electron microscopy and broad spectrum electrochemical impedance spectroscopy (1 Hz–1 MHz) and correlated the physical changes with impedance data to identify markers associated with implant failure.

Main results—RAA produced a diverse range of effects on the structural integrity and electrochemical properties of electrodes. Temperature and ROS appeared to have different effects on structural elements, with increased temperature causing insulation loss from the electrode microwires, and ROS concentration correlating with tungsten metal dissolution. All array types experienced impedance declines, consistent with published literature showing chronic (>30 days) declines in array impedance *in vivo*. Impedance change was greatest at frequencies <10 Hz, and smallest at frequencies 1 kHz and above. Though electrode performance is traditionally characterized by impedance at 1 kHz, our results indicate that an impedance change at 1 kHz is not a reliable predictive marker of implant degradation or failure.

Significance—ROS, which are known to be present *in vivo*, can create structural damage and change electrical properties of MEAs. Broad-spectrum electrical impedance spectroscopy

Online supplementary data available from stacks.iop.org/JNE/12/026003/mmedia

demonstrates increased sensitivity to electrode damage compared with single-frequency measurements. RAA can be a useful tool to simulate worst-case *in vivo* damage resulting from chronic electrode implantation, simplifying the device development lifecycle.

Keywords

neural prosthetics; cortical neural implants; brain–machine interface; microelectrode arrays; accelerated aging; electrochemical impedance spectroscopy; electron microscopy

Introduction

Neural prosthetic systems are medical devices designed to serve as a therapeutic aid to patients with damage to their nervous system. Neural prostheses have been used to provide alternative control capabilities to paraplegic patients (Hochberg *et al* 2006, 2012, Collinger *et al* 2013) and amputees (Dhillon and Horch 2005, Ohnishi *et al* 2007, Raspopovic *et al* 2014). These systems include various types of electrodes that interface with the nervous system and capture multiple types of neural activity, from EMG and EEG population signals to individual single unit action potentials. At present, the use of invasive neural electrodes to capture single unit signals seems to provide the highest-density information content for patient neural prosthetic systems (Wolpaw and Wolpaw 2011). Cortical implants placed in the motor cortex can transmit sufficiently high bandwidth information (Santhanam *et al* 2006) to control sophisticated robotic limbs with many degrees of freedom (Hochberg *et al* 2006, 2012, Collinger *et al* 2013). However, current neuroprosthetic systems raise both safety and efficacy concerns (McGie *et al* 2013a, 2013b). There are several known safety risks inherent to such invasive technology: intracranial surgery involving general anesthesia, penetration of nervous tissue and vasculature by electrodes and subsequent bleeding, the possibility of infection and irritation from the chronic presence of the implant in the brain. In addition, the detection of neural signals declines over time. Within a year from implantation, a decrease in the amplitude of the recorded action potentials (Chestek *et al* 2011) and a drop in the number of active neurons (Kim *et al* 2008) are observed. To be clinically useful, cortical implants should remain functional for much longer periods of time—preferably for the entire life time of the patient. If certain technical challenges can be resolved, leading to improved device safety and efficacy, the performance benefits may outweigh the risks for many patients (Ryu and Shenoy 2009, Wolpaw and Wolpaw 2011, Judy 2012).

Progress in improving neuroprosthetic device reliability is focused on improvement of design and development of new materials for the neural recording electrodes (Judy 2012). Significant efforts have been made to minimize the degree to which penetrating electrodes evoke the brain's foreign body response (Polikov *et al* 2005, Groothuis *et al* 2014). Decreasing implant size is thought to mitigate mechanical damage produced during surgical implantation (Thelin *et al* 2011), reduce vascular damage and elicit a weaker foreign body response during chronic implantation (Bellamkonda *et al* 2013, Karumbaiah *et al* 2013, Saxena *et al* 2013). Decrease in implant size brings a number of engineering challenges. Small probes require small electrodes, which tend to have high impedance outside of optimal recording value. Also, small implants lack the rigidity necessary for tissue penetration during the implantation. Ludwig *et al* demonstrated that coating small electrodes

with PEDOT, a conductive polymer, decreases electrode impedance and results in improved electrophysiological recordings (Ludwig *et al* 2011). Recently, PEDOT was used to coat carbon-fiber microelectrodes and fabricate ultrasmall cylindrical probes with diameters of 8 μm capable of high quality chronic electrophysiological recordings with minimal distortion to blood-brain barrier and reduced reactive tissue response (Kozai *et al* 2012). An alternate strategy is the use of microfabricated probes with lattice structures, which is thought to reduce macrophage activation and decrease the immune response (Seymour and Kipke 2007, Skousen *et al* 2011). Another creative approach is to insulate neurons for the recording from the brain tissue. In this strategy, a glass cone implant with attached gold sensing wires and filled with a neurotrophic factor allowed to sample electrical activity of the newly grown axons inside the cone (Bartels *et al* 2008). In contrast, the use of very soft or biodegradable materials may allow electrodes to integrate into the surrounding tissue more effectively (Ware *et al* 2012, Lind *et al* 2013). For instance, small size flexible probes can be reinforced for insertion with a rigid frame made from a biodegradable carboxymethyl cellulose (Gilgunn *et al* 2012) or silk (Tien *et al* 2013), which dissolves following insertion, leaving a pliable electrode with a small footprint. Similarly, shape memory polymers which transition from rigid to soft state at body temperature are used to fabricate neural implants that are rigid during insertion and soften in the brain to minimize mechanical stress on the adjacent tissue (Ware *et al* 2012).

Novel electrode materials need to be thoroughly tested to assess their safety for use in the nervous system and their capability for effective chronic neural recording. Currently, scientists evaluate the safety and performance of neural implants through chronic implantation in animals. While this approach can provide the necessary preclinical data to demonstrate device reliability and effectiveness, it is expensive and time consuming. An accelerated *in vitro* testing system would allow for more expedient testing of novel electrode strategies, and decrease the device development lifecycle. To address this need, we have developed an *in vitro* system for rapid screening of novel neural implants. Our system simulates degradation of the neural implant that can occur in a stressful environment, such as during chronic implantation in the brain, by using harsher-than-physiological conditions for shorter durations. Medical devices are frequently tested by soaking in saline at an elevated temperature to accelerate the aging process (Fries 2012), and the rates of chemical reactions increase exponentially with increasing temperatures according to the Arrhenius law (Hukins *et al* 2008, Atkins and Paula 2009). However, this approach alone may not adequately capture the aggressive chemical environment that is created by activated immune cells, which release digestive enzymes and reactive oxygen species (ROS) (Badwey and Karnovsky 1980, Halliwell 1992, Polikov *et al* 2005, Freinbichler *et al* 2011, Patrick *et al* 2011). In our system, we have included hydrogen peroxide to mimic the effect of ROS generation during the brain's injury response (Ali *et al* 1993, Zhao *et al* 1995, Patrick *et al* 2011).

In an initial set of experiments, we exposed polyimide insulated tungsten microwire implants to our reactive accelerated aging (RAA) system. Damage observed using electrochemical impedance spectroscopy (EIS) and scanning electron microscopy (SEM) measurements scaled with increases in temperature and hydrogen peroxide concentration, with the most severe degradation caused by aging in high temperature (87 °C) and hydrogen peroxide. We

used these conditions in subsequent experiments to model a ‘worst-case’ degradation process.

To investigate the robustness of various types of neural electrode arrays, we tested four types of commercially available research-grade neural implants (Microprobes for Life Sciences, NeuroNexus, Blackrock Microsystems and Tucker-Davis Technologies (TDT)). To evaluate the impact of the RAA on the implants, we used SEM and EIS.

EIS was used to monitor the change in the absolute value of impedance as well as in phase angle over the full impedance spectrum for frequencies from 1 Hz to 1 MHz. SEM was used to monitor changes in the electrode physical properties, including insulation, metal and substrate materials. We developed novel analysis and data visualization strategies to better represent full spectra EIS data and the characteristic changes found during the aging protocol. We used these analyses to characterize the results of RAA on electrode structural and electrochemical properties, and to investigate the relationship between SEM and EIS changes. Through these data, we identified frequencies that are sensitive to aging processes and examined the correlation between changes in impedance values and structural damage.

Methods

Chemicals

Chemicals were purchased from Sigma-Aldrich (Sigma Aldrich, St Louis, MO) and used as received. Solutions were prepared using deionized water (at 18 MΩ cm).

Cortical neural implants

Neural implants from multiple manufacturers were used in this study (figure S1). Implants were custom ordered to be compatible with an Omnetics Nano 18 channel connector.

Microprobes implants have eight platinum–iridium (70% Pt: 30% Ir) microwires (figure S1(A)). The microwires are coated with Parylene-C and each have a diameter of 75 μm and a nominal impedance of 0.5 MΩ at 1 kHz (Microprobes for Life Sciences, Gaithersburg, MD). Three devices from Microprobes were tested for a total of 24 electrodes.

NeuroNexus implants are a microfabricated 16 channel silicon probes (figure S1(B)) with iridium microelectrode sites, presumably insulated with silicon nitride (Vetter *et al* 2004) and nominal impedance of 1 MΩ at 1 kHz (NeuroNexus, Ann Arbor, MI). Three devices from NeuroNexus were tested for a total of 48 electrodes.

Blackrock Microsystems implants have 16 individual microfabricated silicon needles (figure S1(c)) with Pt-coated tips insulated with Parylene-C and arranged in a 4 × 4 configuration (Blackrock Microsystems, Salt Lake City, UT). The nominal impedance value at 1 kHz for these microelectrodes is about 400 kΩ. One Blackrock device was tested for 16 electrodes total.

TDT implants consist of an array of 16 polyimide insulated gold-coated tungsten microelectrodes (figure S1(D)) with diameter of 50 μm and impedance of 15 kΩ at 1 kHz (TDT, Alachua, FL). Four TDT devices were used to test RAA system at different

conditions. Finally, three more devices from TDT were tested using the final RAA system, for a total of 48 electrodes.

Reactive accelerated aging (RAA) system

A jacketed flask (Pine Research Instrumentation, Durham, NC) equipped with six 24/40 ports and one 40/35 center port was used as a RAA reactor. The flask was connected to a Haake C-25 circulator with mineral oil (Fisher Scientific, Pittsburgh, PA). The thermostat temperature was set slightly higher (94 °C) than the desired temperature for RAA to compensate for heat loss. The flask was covered with dark cloth (Thorlabs, Newton, NJ) to prevent light interference with the reaction. The neural implants were fixed on the holder and lowered in the reaction media. The holder was constructed using an Omnetics based printed circuits board (PCB) board adapter from TDT. The experimental procedure is outlined in scheme figure 1(A) and the RAA system is shown on figure 1(C).

Maintaining hydrogen peroxide concentration

For the given conditions, we observed that kinetics of hydrogen peroxide degradation at elevated temperature (87 °C) follows first order kinetics with a half-life of 23 min. Repeated injections of concentrated hydrogen peroxide solution were employed to maintain a concentration in the reactor in the range of 10–20 mM. Samples were taken several times per day from the reactor for each experiment to ensure that the concentration of hydrogen peroxide was maintained within the desired limits. Injection parameters such as concentration of hydrogen peroxide in injectable solution, pumping rates, duty cycles for the both injection and drain pumps were adjusted to maintain the appropriate concentration of hydrogen peroxide.

At the beginning of the RAA experiment, 750 mL of 20 mM hydrogen peroxide in PBS solution was placed in the flask. During the experiment, a Watson-Marlow 401 U/DM3 peristaltic pump (Watson-Marlow Pumps, Wilmington, MA) was used to deliver concentrated hydrogen peroxide solution (750 mM in PBS buffer) at a rate of 0.5 mL min^{-1}. The pump was controlled through a timer (Talento-121, Intermatic, Spring Grove, IL) that operated in 2.5/12.5 min ON/OFF duty cycle. The solution level was kept constant by removing excessive fluid with a vacuum pump to a waste reservoir. The vacuum pump was connected to a mechanical analog timer, which operated with a 15/225 min ON/OFF duty cycle. Concentration of the delivered hydrogen peroxide solution, duty cycle of the pump and the pump rate were adjusted during each individual run to ensure that the concentration hydrogen peroxide is maintained within 10–20 mM.

Hydrogen peroxide assay

Samples of the solution were periodically taken from the RAA flasks (0.5 mL) and stored in the fridge. Samples were analyzed for hydrogen peroxide using a previously described titanium oxalate assay (Eisenberg 1943). Briefly, 50 μL of the sample was mixed with 200 μL of 1.0 M H_2SO_4, 200 μL of titanium potassium oxalate (50 g L^{-2}) and diluted to 5 mL with deionized water. Solution was left for 5 min for reaction to complete. UV–vis spectra were taken and absorption at 390 nm was measured with an Agilent 8453 spectrophotometer (Agilent Technologies, Santa Clara, CA).

Electrochemical impedance spectroscopy (EIS)

EIS was performed with a Gamry Reference 600 potentiostat (Gamry Instruments, Warminster, PA). The measurements were done in phosphate buffered saline, pH 7.4, at ambient conditions. Impedance was measured in a two-electrode scheme with a 10 mm long Ag/AgCl wire used as a counter/reference electrode. A perturbation voltage with amplitude of 25 mV was used in the frequency range of 1 Hz–1 MHz, with 5 frequency points per decade. No dc offset in respect to the open circuit potential was used.

Full spectra EIS data for the implants are plotted in two formats. Traditional Bode plots of impedance absolute value and phase angle versus frequency are accompanied with pseudocolor plots. Pseudocolor plots are geometrically arranged two-dimensional color coded plots of either impedance or phase values with frequency on the abscissa and electrode number on the ordinate. The impedance traces in a pseudocolor plot matched the arrangement of the electrodes in the implant.

Scanning electron microscopy (SEM)

Neural implants were thoroughly rinsed for several minutes with a stream of deionized water to remove salt deposits. Electron micrographs were obtained with a JEOL JSM-6390LV scanning electron microscope (JEOL USA, Peabody, MA) in low vacuum mode with electron acceleration potential of 15 kV and pressure of 30 Pa. These conditions allow imaging of neural implants without the artifacts related to ‘ charging’ effects from the electron beam.

Inductively coupled plasma mass spectrometry (ICP-MS)

Samples of the liquid collected for hydrogen peroxide assay during TDT neural implants aging were analyzed for presence of tungsten using ICP-MS (figure 1(A)). 0.1 mL of sample solution was diluted to 5 mL with 2% nitric acid and analyzed using Thermo Scientific × series 2 ICP-MS (Thermo Scientific, Waltham, MA).

Software and data analysis

The averaged data are presented as mean with the standard deviation. Impedance data were collected and analyzed using Gamry Instruments software. Data were processed and plots were generated using MATLAB (Mathworks, Natick, MA), MS Excel (Microsoft, Redmond, WA) and Origin (OriginLab Corporation, Northampton, MA). Images were processed using ImageJ (Schneider *et al* 2012) to measure change in electrode area after RAA.

Results

Effects of elevated temperature and ROS on electrode integrity

To define the contributions of each component of our RAA protocol, we investigated the differential effects of temperature and ROS on polyimide-coated tungsten microwire arrays (TDT). TDT arrays were aged at temperatures 37 °C and 87 °C in PBS with and without hydrogen peroxide for 7 days. Dissolution of tungsten in the reactor was monitored twice daily using ICP-MS (figure 1(B)). Concentration of tungsten is proportional to tungsten

dissolution rate and thus is a quantitative marker for the degradation process. The fastest dissolution of tungsten was observed with RAA at 87 °C in presence of 20 mM of hydrogen peroxide with a peak tungsten concentration of 1.28 ppb. The second most rapid dissolution was at 37 °C in presence of hydrogen peroxide with a peak tungsten concentration of 0.34 ppb. The dissolution in PBS without hydrogen peroxide was more moderate with the slowest rate at 37 °C (peak tungsten concentration 0.051 ppb) and a slightly higher rate at 87 °C (peak tungsten concentration 0.071 ppb). Electron microscopy of the aged TDT arrays demonstrated subtle changes for the implant aged at 37 °C in PBS (figure S2(A), (S) refers to figures 'supplementary materials') and in presence of hydrogen peroxide (figure S2(C)). Almost no flaking of insulation and minor to moderate dissolution of tungsten is visible in both conditions (figures S2(A1)–S2(A2) and S2(C1)–S2(C2)). Substantial loss of insulation was observed for aging at 87 °C in PBS (figures S2(B) and S2(B1)–S2(B2)) and complete loss of insulation with tungsten dissolution and bending of the electrodes is observed for RAA at 87 °C in hydrogen peroxide (figures S2(D) and S2 (D1)–S2(D2)). EIS showed a slight decrease in impedance magnitude in region from 1 to 100 Hz (63 ±5% at 10 Hz, averaged for 16 electrodes) for TDT implants exposed to PBS at 37 °C (figure S3(A)). Aging in PBS at 87 °C lead to a less uniform EIS response (figure S3(B)) with a decrease in impedance magnitude over 1 to 100 Hz (34 ±18% at 10 Hz, averaged for 16 electrodes) as well as a considerable drop at the region from 10 kHz to 1 MHz (87 ± 2% at 1 MHz, averaged for 16 electrodes). Aging in the presence of hydrogen peroxide at 37 °C led to greater dispersion of impedance values (from 11.6±1 kΩ to 18.5 ± 7 kΩ at 1 kHz, averaged for 16 electrodes), but did not lead to a trending change in impedance for most of the electrodes, although impedance increased for two electrodes in 10 kHz to 1 MHz region (figure S3(C)). RAA at 87 °C in hydrogen peroxide lead to a decrease in impedance magnitude over the 1 to 300 Hz region (figure S3(D)) and increase in variability of impedance over the region from 1 kHz to 1 MHz with decrease in impedance (8 electrodes), increase in impedance (5 electrodes) and lack of particular trend (3 electrodes) for different groups of electrodes.

RAA of neural implants with different designs

After defining the RAA parameters that produce the most robust change in materials integrity, we applied this protocol to multiple commercially-available research-grade multielectrode arrays designed for implantation in the brain. We chose arrays that are widely used in the research environment, and encompass a range of design and materials specifications. Accordingly, we selected micro electrode array (MEA) (MEA, Microprobes for Life Sciences), Utah Array (Blackrock Microsystems), Neural Probe (NeuroNexus), and microwire arrays (TDT). The MEA, Utah Array and TDT array have individual penetrating shanks for each electrode contact, while the Neural Probe has multiple electrode contacts on a single penetrating shank. The MEA and TDT array are composed of individual microwires for each electrode, while the Utah array and Neural Probe are fabricated using a silicon substrate. The MEA comprises platinum/iridium microwires for the conductive element, insulated with Parylene-C, while the TDT array comprises tungsten microwires surrounded by a gold sheath, and has polyimide insulation. The Utah array comprises platinum conductive elements, which are insulate has Parylene-C dielectric. Meanwhile, the NeuroNexus Neural Probe comprises iridium conductive elements and a silicon compound

dielectric for frame and insulation. We exposed each of these array types to the harshest RAA protocol, with 7 days submersion in 20 mM hydrogen peroxide at 87 °C. Arrays were fully characterized with EIS and SEM microscopy before and after RAA protocol.

RAA of Microprobe implants

The effect of RAA varied from implant to implant for Microprobes. For one implant ($N = 8$ electrodes, all on the same implant), electron microscopy did not reveal any substantial changes in appearance of platinum/iridium metal microelectrode tips or the Parylene-C insulation (representative electrode figures 2(A) and (D)). For the other group ($N = 8$ electrodes, three on one implant and five on the other implant) of electrodes, changes in the structure of Parylene-C at the tips were observed with the insulation receding and exposing the larger electrode area (representative electrode figures 2(B) and (E)). Finally, for a group of electrodes ($N=8$ electrodes, five on one implant and three on the other implant), insulation accumulated at the tips and lead to either partial or full coverage of the electrode metal tips (representative electrode figures 2(C) and (F)).

The implant that did not show any substantial change in electrode morphology under the microscope also demonstrated a small drop in impedance, while the other two implants showed large decreases in impedance across all frequencies (figure 2(G)). Similarly, an increase in phase angle was more substantial for two implants that experienced changes in insulation structure (figure S4(A)). Both pseudocolor plots for impedance magnitude (figures 2(H) and (I)) and phase shift (figures S4(B) and S4(C)) revealed spatial clustering: electrodes 1–4 demonstrated observable decreases in impedance at low frequencies (1 Hz–1 kHz), while electrodes 5–8 did not. Phase angle increased for electrodes 1–4 more than for electrodes 5–8 (figures S4(B) and S4(C)). The clustering was not observed for the other two implants.

RAA of NeuroNexus implants

Electron microscopy did not reveal any observable change in the appearance of the NeuroNexus implants after RAA (figures 3(A)–(D)) ($N=48$ electrodes, three arrays). However, EIS revealed a significant decrease in impedance over all frequencies for one of the arrays. For the other two arrays, impedance decreased significantly over the frequency 1 Hz– 10 kHz, slightly increased at 100 kHz and did not change at 1 MHz (figure 3(E)). Phase angle increased over the 1 Hz– 100 kHz region for all implants, but it dropped in 100 kHz– 1 MHz region for two implants (figure S5(A)).

Pseudocolor plots did not show any spatial clustering for impedance magnitude (figures 3(F) and (G)) or phase shift (figures S5(B) and S5(C)), but did reveal an alternating pattern in impedance for electrodes 3–14 visible at frequencies from 10 Hz to 100 Hz, which was preserved after RAA.

RAA of Blackrock implant

Electron microscopy did not reveal significant changes in the appearance of the Blackrock arrays after RAA (figures 4(A) and (B)) ($N = 16$ electrodes, one array). Some slight alterations in a form of peeling of Parylene-C insulation can be seen on the frame of the

implant (figures 4(C) and (D), white arrow). There was no observable difference in the insulation on the electrode tips at high magnification (inset to figures 4(A) and (B)).

Impedance spectroscopy demonstrates significant drop in the electrode impedance at all frequencies (figure 4(E)). Except for one outlier (electrode 2, figure 4(F)), the impedance spectra are very similar between the electrodes, and the impedance uniformly dropped after RAA for all the electrodes. Following RAA, the impedance of the outlier dropped to a magnitude comparable to the other electrodes (figure 4(E) and electrode 2 on figures 4(F) and (G)). Changes in impedance magnitude (figures 4(F) and (G)) and phase (figure S(6)) do not show any topological clustering associated with changes after the RAA.

RAA of TDT implants

Electron microscopy revealed signs of degradation on TDT implants following RAA (figures 5(A) and (B)) (N=48 electrodes from three arrays). Apparent delamination of polymeric insulation was accompanied by etching and dissolution of tungsten wires within the remaining gold sheath. Higher magnification images show tungsten metal dissolved from the core of the electrodes, leaving only hollow gold tubes (inset to figure 5(B)). These gold tubes are very fragile and a number were bent or broken.

The visible deterioration in electrodes coincided with decreased impedance at low (1 Hz-100 Hz) and high frequencies (100 kHz-1 MHz) range for all arrays (figure 5(C)). There was no significant change in frequencies surrounding 1 kHz. The phase angle increased at 1 Hz-1 kHz range and slightly decreased at frequencies between 100 kHz and 1 MHz (figure S7(A)).

Full spectra pseudocolor plots showed some clustering with higher impedance for the electrodes (2, 3, 7 and 8) at high frequencies (1 kHz–1 MHz), but not for any electrodes from 9 to 16 (figures 5(D) and (E)). The same pattern is observed for the phase angle with electrodes 2, 3, 7 and 8 having lower phase angle values at high frequencies (1 kHz–1 MHz), but not for electrodes from 9 to 16 (figures S7(B) and S7(C)).

Because overt structural damage was observed in these electrode arrays following RAA, we were able to investigate the correlation between the degree of structural damage and changes to the impedance spectrum on a single-electrode scale. We first quantified structural integrity, and then compared that to the impedance at a commonly-used measurement frequency, 1 kHz. The electrode with the largest increase in the impedance at 1 kHz (figure S8(E)) had 92% insulation loss (electrode **e**, figure S8(B)), while the electrode with the largest decrease in the impedance at 1 kHz (figure S8(C)) had only 21% insulation loss (electrode **c**, figure S8(A)). Alternatively, both an electrode with 80% insulation loss (electrode **d**, figure S7(A)) and an electrode with only 15% insulation loss (15%, electrode **f**, figure S8(B)) did not experienced any change in the impedance at 1 kHz (figure S8(D)). Over all electrodes, we found no correlation between insulation loss and impedance change at 1 kHz (figure 6(E)).

Trends in change of electrode morphology and electrode impedance

Electron microscopy revealed changes in electrode morphology after RAA for Microprobes and TDT implants. These transformations included change in the exposed electrode area. We quantified this change for all electrodes and compared it with the change in electrode impedance at three frequencies: 10 Hz, 1 kHz and 100 kHz (figure 6). Correlation coefficients were small for all implants and all electrodes ranging from R^2 of 0.0005 (TDT at 100 kHz, figure 6(D)) to R^2 of 0.0463 (Microprobes at 100 kHz, figure 6(A)).

To compare changes in the magnitude of impedance across all four neural implant types, we calculated the change in impedance relative to the starting impedance, across the frequency spectrum and displayed it on a log-log axis (figure 7). These plots reveal the frequencies at which the magnitude of the impedance is the most sensitive to the accelerated aging process. The dynamics of this frequency dependence differ between the four different implants. For the Microprobes MEAs (figure 7(A)), the change in electrode impedance after RAA was the most significant at low frequencies with an impedance decrease, log (Z_{post}/Z_{pre}) of –1.9 ± 1.0 at 1 Hz and a corresponding decrease in variance. At 1 kHz the impedance change was −1.2 ±0.9. For the NeuroNexus implants (figure 7(B)), the greatest change in the impedance occurred at frequencies below 1 kHz, with the frequency range from 1 to 10 Hz showing impedance drops of nearly three orders of magnitude. The Blackrock MEA (figure 7(C)) had the largest overall reduction in impedance, with a drop greater than a three orders of magnitude for frequencies from 1 Hz to 10 Hz, and lesser reductions across the entire spectrum. TDT MEAs (figure 7(D)), had the smallest overall change in impedance, with significant changes in impedance at low frequencies (1 –10 Hz) and high frequencies (>10 kHz). At 1 kHz, the impedance change log (Zp_{ost}/Zp_{re}) was −0.43 ± 0.42, meaning that this change is very inconsistent from electrode to electrode.

Discussion

Regulatory perspective

Invasive neural implants designed for recording neural signals over chronic (>30 days) timescales have not yet been brought to market in the US. Given the potential risks inherent in implanting electrodes into neural tissue, it is likely that many future neural implant devices will be considered high-risk, and may need to follow the FDA’ s premarket approval (PMA) process for regulatory approval (Welle and Krauthamer 2012). PMA submissions must demonstrate a reasonable assurance of safety and effectiveness using valid scientific evidence provided through bench testing, animal studies and clinical trial data. Bench testing is often the first, and typically the least resource-intensive portion of the testing process, and can eliminate the need for some future animal or clinical trial data. It can also address questions regarding maximum limits that cannot be addressed by clinical or animal studies. Thus, the development of a rapid *in vitro* evaluation method to determine device robustness design could be beneficial. A thorough study of the assembled device should provide data on possible failure modes; spot the weak points in the device design, and should include the development of analytical methods to trace the markers that can be used to predict the device failure. Multiple factors may contribute to the decline of cortical implant performance; they can be broadly classified as either ‘biotic’ or ‘abiotic’ failures (Sanchez *et al* 2006). Biotic

failure includes death of neurons near the implant (Biran *et al* 2005, McConnell *et al* 2009) and gliotic encapsulation of the implant that may prevent sensing of action potentials (Rousche and Normann 1998, Roitbak and Syková 1999, Polikov *et al* 2005). Abiotic failure manifests as degradation of the implant which includes but is not limited to corrosion of metallic electrodes, (Sanchez *et al* 2006, Prasad *et al* 2012), decomposition and delamination of electrode insulation (Schmidt *et al* 1988, Sanchez *et al* 2006, Barrese *et al* 2013), and damage and degradation of connector and the implant body (Schmidt *et al* 1988, Simeral *et al* 2011, Barrese *et al* 2013). Future advancement in cortical neuroprosthetics relies on the advances in design of the neural implants that are resistant to this decline in performance.

Reactive accelerated aging system

Accelerated aging is traditionally performed in a buffer solution at elevated temperature, which increases the rates of chemical reactions that degrade the device (Hukins *et al* 2008). The assumption is that the same reactions take place at body temperature as at the elevated temperature. However, the *in vivo* environment has additional chemical reactions that are not taken into account by current testing protocols. Immune cells attack implants *in vivo* by releasing ROS that are not present in a saline solution. Previous work has simulated *in vivo* degradation in the presence of these chemicals by including hydrogen peroxide (Meijs *et al* 1993, Yokoyama *et al* 2007, Patrick *et al* 2011) or generating reactive species *in situ* via the reaction of hydrogen peroxide with the metal ions in aging protocols (Ali *et al* 1993, Zhao *et al* 1995). One of the challenges of including ROS is their short lifetimes. This makes it difficult to assure reproducible exposure to targeted concentrations of peroxide for a specified period of time. While some of the previous studies were able to simulate *in vivo* conditions in some cases (Meijs *et al* 1993, Patrick *et al* 2011), they used hydrogen peroxide levels far above physiological levels. For example, the concentration of hydrogen peroxide used was as high as 8 M (Meijs *et al* 1993), which is well above than the concentration of hydrogen peroxide *in vivo*, around 0.1 μM (Giorgio *et al* 2007) and above the concentration of hydrogen peroxide that is reported to induce oxidative stress, around 1 mM (Chichili *et al* 2006). Previous attempts to simulate the impact of ROS *in vivo* were also limited by the lack of control of hydrogen peroxide concentration. Hydrogen peroxide degrades at high temperature, necessitating continuous monitoring and replenishment. We decided to use 10–20 mM of H_2O_2 to simulate a worst-case scenario of reactive oxygen stress.

In this work, we designed a RAA system to evaluate the durability of implantable neural devices under an extreme biological stress. This protocol is simple, inexpensive and easy to replicate. The most sensitive component of the system is the mechanism for injecting hydrogen peroxide to maintain the desired concentration of peroxide. The hydrogen peroxide concentration is routinely monitored and a timer-controlled pump delivers fresh hydrogen peroxide solution. We used this system to test four widely used commercial neural implants of different design. To evaluate the impact of our RAA system, we applied two analytical techniques for characterizing devices; SEM and EIS. These techniques were chosen because of the versatility with which they can be applied to in *vitro, in vivo* and *post vivo* situations, allowing for direct comparisons between real and simulated aging. Patrick *et al* used these techniques to study tungsten neural implants *in vitro, in vivo* and *post vivo* (Patrick *et al* 2011). Our work expands this approach by using broad spectrum impedance

spectroscopy together with electron microscopy to investigate the impact of RAA on implants of different design and materials. In this way, we aim to develop a comprehensive platform to assess reliability of neural implants.

To verify that the chosen conditions lead to quick degradation of neural implants, we performed RAA experiments with TDT MEAs and varied the temperature and presence of hydrogen peroxide during the experiment. As demonstrated in earlier studies, tungsten dissolves in buffer solution (Peuster *et al* 2001, Sanchez *et al* 2006) and we find this process is facilitated by the presence of hydrogen peroxide. The rate of this process was quantified with elemental analysis technique (ICP-MS). Our results indicate that the slowest dissolution rate of tungsten was observed in PBS at 37 °C followed by dissolution at 87 °C in PBS. Faster dissolution rates were observed in presence of hydrogen peroxide at 37 °C and the fastest rate was achieved in the presence of 87 °C with hydrogen peroxide. Based on these data, we suggest that hydrogen peroxide seems to be a driving factor for tungsten dissolution as compared to temperature. Loss of polyimide insulation was also observed during RAA. Based on SEM imaging, the least polyimide insulation was lost at 37 °C in both PBS and hydrogen peroxide, without a clear difference between these two conditions. Greater loss was observed at 87 °C in PBS, with the greatest loss occurring at 87 °C in hydrogen peroxide. The EIS demonstrated the least change in impedance for 37 °C in both PBS and hydrogen peroxide. In the presence of hydrogen peroxide, the impedance increased at higher frequencies for several electrodes which might be explained by greater dissolution of tungsten electrodes at these conditions. The drop in impedance for TDT implants aged at 87 °C in PBS is uniform among electrodes and probably associated with delamination of polyimide insulation that is observed with SEM. Change in EIS spectra after RAA at 87 °C in hydrogen peroxide is less homogeneous. The drop in impedance magnitude at lower frequencies is uniform and probably indicative of polyimide insulation removal. Additionally, based on SEM insulation delamination is accompanied by dissolution of tungsten and breaking and bending of the gold coating on the electrodes which are both the factors contributing to the increase in impedance and are likely responsible for high variability among the results. Overall, it seems that increase in temperature is an important factor for degradation of polyimide insulation, while the presence of hydrogen peroxide leads to much quicker dissolution of tungsten.

Based on these preliminary results, we elected to perform all subsequent RAA protocols at 87 °C in hydrogen peroxide to create a ‘worst-case’ accelerated aging environment that could cause damage to the polymer dielectric and metallic conductive elements. This protocol was applied to microwire multielectrode arrays (Microprobes, Tucker-Davis Technology) and silicon substrate arrays (NeuroNexus, Blackrock Microsystems).

Impact of the RAA

Exposure of neural implants from Microprobes to RAA produced varied results across the arrays. Electrodes from one array did not show any noticeable structural changes in electron micrographs. Electrodes from the two other arrays showed shifts in the location of the Parylene-C insulation, which appeared to have moved with respect to the electrode, either exposing more of the electrode tip, or covering the electrode contact surface entirely.

Electrodes with this morphological change also demonstrated a decrease in the absolute value of impedance and an increase in phase angle for frequencies lower than 100 kHz. The impedance dropped from 2.0 ± 1.2 MΩ to 0.35 ± 0.49 MΩ at 1 kHz, but changed little for higher frequencies between 100 kHz and 1 MHz. The drop at low frequencies might be due to delamination of insulation from the electrode metal surface or moisture penetrating through the Parylene-C, causing a switch from a more capacitive to a more resistive conductivity mode which is manifested as an increase in the phase angle at low frequency. Davis *et al* described such moisture diffusion in Parylene-C (Davis *et al* 2011). Furthermore, water diffusion through parylene leads to an increase in dielectric permittivity and capacitive coupling through the insulation (Seymour *et al* 2009). In addition, we performed our RAA experiments at temperatures higher than the glass-transition point for Parylene-C (~60 °C). At these conditions, the material develops cracks and pin-holes. Both processes lead to a decrease in electrode impedance.

An arrangement of the impedance data into pseudocolor plots revealed a topological structure of the impedance changes. In one Microprobes array, electrodes one to four showed greater decrease in impedance at lower frequencies compared to electrodes five to eight. In Microprobes implants, the electrodes are arranged in two groups of four electrodes on two PCBs boards. Uniform decrease in the impedance for the electrodes located on the same PCB suggest that there is some failure of insulation and possible ingress of moisture that affects all electrodes on this board.

RAA of NeuroNexus neural implants did not result in any change in appearance in the electron micrographs, but produced a significant drop in impedance and increase in phase angle at lower frequencies. The impedance at 1 kHz droped (1.2 ±0.3 MΩ to 0.19 ±0.21 MΩ), while impedance at 1 MHz changed little on average (18 ± 2 kΩ to 14 ± 8 kΩ) but showed increased variability between the electrodes. These changes may indicate a switch from capacitive to resistive conductivity mode that could be due to increased electrode area, cracks in the insulation, or the formation of iridium oxide. If hydrogen peroxide oxidizes iridium to form iridium oxide, this can lead to a decrease in charge transfer resistance. In this case, the impedance at lower frequencies will be dominated by the charge transfer at the electrode surface.

Blackrock arrays showed slight alterations in morphology of insulation on the frame of the array. However, no major signs of insulation rupture were observed at high magnification at the electrode tips. The impedance of the electrodes decreased significantly at all frequencies. The decline was considerable: at a frequency of 1 kHz; with the impedance drop from 600 ± 200 kΩ to 10± 8.0 kΩ. The phase angle increased at all frequencies, indicating that the resistive mode of conductivity dominates. Pseudocolor plots did not expose any patterns associated with the spatial arrangement of the electrodes in the array.

Since both Blackrock and Microprobes arrays are insulated with Parylene-C, it is likely that the same process, such as diffusion of the moisture through the Parylene-C insulation (Davis *et al* 2011), could have led to the drop in impedance. For example, the impedance for one Blackrock electrode was much higher than the average (5.7 MΩ at 1 kHz) and after RAA dropped to the same level as other electrodes. The phase shift for this electrode was also

lower than it was for other electrodes, indicating a capacitive mode of conductivity. The impedance dynamics for this electrode may be explained by moisture diffusion. Moisture accumulation under Parylene-C insulation at the connection to electrodes would provide an alternative current pass and lead to a drop in the electrode's impedance.

Microelectrodes of the TDT neural implant showed significant degradation in our test system. Polyimide insulation disintegrated and peeled off of the microwires. Additionally, the wires corroded with the complete dissolution of tungsten, leaving behind hollow gold tubes. Degradation of insulation increased electrode surface area, which should increase capacitance, decrease resistance, and decrease electrode impedance at all frequencies. However, the corrosion and etching of the tungsten electrode should have the opposite effect. As a result, the pattern of impedance changes was unpredictable: on average, impedance dropped both at low frequencies from 499 ± 243 kΩ to 54 ± 47 kΩ at 10 Hz and at high frequencies from 3.2±0.9 kΩ to 0.76 ± 0.69 kΩ at 1 MHz. However, there is a very slight change in impedance at 1 kHz, where it decreases from 14.6 ± 6.5 kΩ to 6.9±7.3 kΩ with large spread in the direction and magnitude of the impedance for the aged implants. The phase data show more capacitive conductance for the frequency in 1 Hz–1 kHz range for the aged implants.

Overall, for Microprobes, Neuronexus and TDT implants we observed considerable variability between electrodes on a single array following RAA. For Microprobes and TDT implants, the variability observed in the structural response to aging may be due to minute differences in the electrode manufacturing process, for example, the deinsulation process of electrode contacts. While TDT and Microprobes are made with polymer insulated metal wires, Neuronexus and Blackrock arrays are made using lithography and microfabrication techniques. Neuronexus arrays exhibited alternating patterns in impedance magnitude, both before and after RAA, indicated perhaps some systematic variability related to the electrode design. Unlike the other electrode styles, variability in impedance was reduced for Blackrock arrays following RAA due to uniform profound drop in impedance magnitude for all electrodes.

Electrochemical impedance spectroscopy for evaluation of implant failure

EIS is the only technique for routine electrochemical evaluation of the microelectrodes *in vivo*. However, published investigations have not yet been able to provide a conclusive link between changes in EIS and a correct prediction of electrode failure *in vivo*. The time course of *in vivo* EIS dynamics has been well characterized, and shows common characteristics across various electrode materials and animal model species. *In vivo* increases in impedance occurring during the first 2–3 weeks following implantation have been reported for microfabricated silicon or polyimide arrays (Rousche and Normann 1998, Mercanzini *et al* 2009, Simeral *et al* 2011, Barrese *et al* 2013, Malaga *et al* 2014) and wire arrays (Schmidt *et al* 1976, Lempka *et al* 2009, Prasad *et al* 2012) in studies conducted in rodents (Mercanzini *et al* 2009, Prasad *et al* 2012), non-human primates (Barrese *et al* 2013, Malaga *et al* 2014) and human patients (Simeral *et al* 2011). At times longer than 30 days post-implantation, impedance either appears to plateau (Vetter *et al* 2004, Mercanzini *et al* 2009, Prasad and

Sanchez 2012) or to gradually decrease over the subsequent months and years *in vivo* (Schmidt *et al* 1976, Rousche and Normann 1998, Branner *et al* 2004, Barrese *et al* 2013).

In vivo changes of impedance spectra are frequently ascribed to dynamics of the local tissue environment. The time course of a typical tissue response to electrode insertion shows an acute response characterized by widespread astrocytic and microglial activation and brain edema, followed in several weeks by a retraction of the glial response to a tight ring around the electrode (Szarowski *et al* 2003, Polikov *et al* 2005, Spataro *et al* 2005). Encapsulation by glial cells can increase local tissue resistance (Grill and Mortimer 1994, Moffitt and McIntyre 2005), and correspondingly, the initial transient increase in impedance has been shown to depend on the intensity of the local neuroinflammatory reaction (Williams *et al* 2007, McConnell *et al* 2009). Long-term impedance reductions are less closely linked to histological outcomes.

Neuroinflammatory markers in rodents implanted for up to 9 months showed milder expression at late time points than during the acute phase, suggesting that chronic neuroinflammation alone is not solely responsible for a decline in device performance (Prasad *et al* 2012). Likewise, the timeframe for the stabilization of the glial response occurs over weeks to months post-implantation, while the progressive impedance decline occurs over months to years, a discrepancy noted in an analysis of failure mechanisms of arrays implanted in non-human primates (Barrese *et al* 2013). These authors, and others (Rousche and Normann 1998, Branner *et al* 2004), have suggested that shunting due to water permeation into the system could instead play a major role in later impedance declines.

Our RAA test platform is designed to simulate electrodes that have experienced roughly 6 months implantation *in vivo*. Electrodes that have been ‘aged’ in this system show a decrease in impedance measured at frequencies of 1 kHz or less, regardless of electrode material or form factor. These results are consistent with the decrease in impedance observed in the long-term *in vivo* implantation studies mentioned previously. Given our analysis of impedance and phase changes, we propose that much of the decreased impedance is due to compromise of the electrode insulation integrity. This supports the hypothesis that *in vivo* impedance declines seen at later time points might be related to changes in the material properties of the electrode, rather than ongoing inflammatory responses. A thorough evaluation of explanted electrodes using EIS and surface microscopy techniques, and comparison to pre-implantation and *in vivo* measurements would help to elucidate the influence of material changes on electrochemical properties of implanted electrodes.

Researchers have routinely measured impedance at 1 kHz to characterize the electrode performance for electrophysiological recordings (Ludwig *et al* 2006, Ward *et al* 2009, Simeral *et al* 2011, Prasad *et al* 2012). The frequency of 1 kHz matches the frequency of the neural action potential, which is about a millisecond long (Humphrey and Schmidt 1990). This means that the current produced by a neuron during firing of the action potential has the same ability to penetrate the surrounding media to reach the recording electrode as the current generated during the impedance measurements (Ludwig *et al* 2006). However, it is unclear whether impedance magnitude at 1 kHz can accurately predict the degradation of neural implants associated with abiotic failure. In our study we acquired full spectra EIS

data for the implants before and after degradation to explore the capability of other frequency ranges to predict damage to the electrode arrays produced by RAA.

The full impedance spectra measurements provide a more comprehensive picture of the impedance change than single measurements at 1 kHz. Particularly, for the TDT implants, impedance at 1 kHz does not have a clear trend that would predict the malfunctioning of the implant, despite the obvious degradation shown with electron microscopy. When we compared two electrodes with different degree of the delamination of insulation, the impedance at 1 kHz was very similar and did not change significantly from the pre-aging value. Furthermore, it did not correlate with the degree of insulation loss. However, at high frequencies, the decrease in impedance was greater for the electrode with complete elimination of the insulation, illustrating the advantage of the full spectra impedance spectroscopy for the evaluation of neural implants.

One particular challenge for using EIS with a wide frequency range is the large amount of data generated for each neural implant. For the given conditions, there are up to 960 data points per implant with sixteen electrodes. For an implant with one hundred electrodes that is used in clinical trials this number would reach 6000 data points. The pseudocolor coding of impedance data implemented in this work provides a rapid snapshot of the implant state and is complementary to the standard two-dimensional Bode plots. This approach was previously used for representing electrochemical data for fast-scan cyclic voltammetry (Michael *et al* 1998). Impedance data is plotted in a geometric arrangement that matches that of the electrodes in the implant. This orientation helps to establish any correlation in the change of impedance that might be relevant to the design of the implant. Particularly, pseudocolor plots for impedance of Microprobes and TDT neural implants after the RAA suggest that the impedance changes are different for the electrodes that are located on different printed circuit boards and on different sides of the Omnetics connector. This finding suggests that RAA affects either the boards or the connector. Hence, this information could be used to suggest a possible mechanism of failure for the implant.

The best frequency for monitoring implant degradation is the frequency that gives the greatest change in the impedance (highest sensitivity) with the smallest standard deviation (highest precision). Based on our data for the Microprobes neural implants, this would be a low frequency (1 –10 Hz) where the change in electrode impedance after RAA was the most significant. 1 kHz would be less suitable since the standard deviation at this frequency is high. The same is true for NeuroNexus implants where the greatest change in the impedance with the smallest standard deviation occurred at low frequencies (1 –10 Hz). The impedance change at frequencies at and above 1 kHz had high standard deviation which means it is imprecise marker for the changes in the state of the implant. The Blackrock MEA had a significant drop in the impedance over the entire range of frequencies, however, the highest drop was observed at low frequencies from 1 to 10 Hz. For the TDT MEA, the most reliable prediction of degradation is change at low frequencies from 1 to 10 Hz. The change in impedance at 1 kHz has high standard deviation which means it is very inconsistent from electrode to electrode, and is difficult to make predictions regarding the state of the electrode materials.

This analysis reveals that the dynamics of impedance change across different implants is unique to the specific implant, and thus monitoring of the impedance at 1 kHz is not necessarily the best marker for implant failure and degradation. However, across all electrode arrays, the impedance <10 Hz seems to be most sensitive to aging procedures, regardless of any observed physical damage.

Conclusions

We developed a RAA system for the rapid simulation of the 'worst case' *in vivo* environment for cortical neural implants. We used this system to investigate the effects of accelerated aging of commercially-available, research-grade cortical neural implants from Microprobes, NeuroNexus, Blackrock Microsystems and TDT. Electron microscopy revealed signs of structural degradation for TDT, Microprobes and Blackrock electrodes, but not for NeuroNexus arrays. Impedance values dropped for all arrays, and decline in the low (<1 kHz) frequency range was consistent across all array types. A decline in impedance after a simulated 6 months *in vivo* is consistent with published reports on *in vivo* impedance changes. Declines in other frequency ranges may provide array-type-specific information about aging. Phase data combined with impedance data suggests a shift from reactive to capacitive processes, which is consistent with a scenario in which the insulation barrier is compromised. In most cases, changes in electrical impedance spectroscopy were not closely associated with structural deficits in a predictable manner. In fact, the TDT implant showed that the impedance change at 1 kHz does not provide a reliable marker for the state of the implant. The change in the impedance observed at 1 kHz for the TDT electrodes was not significant, but the electrodes showed profound degradation. Taken together, these results make a strong case for the use of full spectra EIS to provide more comprehensive data on aging process of neural implants.

We find that pseudocolor plot representation of EIS data allows for easy comparison across electrode arrays, and can reveal structural trends in array aging. This feature allowed us to observe examples where impedance change seems to segregate based on PCB board connections, suggesting that liquid penetration may occur at the level of the electrode PCB board or connector.

We described a simple and robust platform for comprehensive study of the reliability of neural implants that incorporates reactive elements like those found in the brain microenvironment. The analytical techniques, full spectrum EIS and SEM, can be used in *in vivo* and *post vivo* analyses to validate *in vitro* findings. Our results indicate that although impedance change can result from the aging process, the correlation between impedance change and structural damage is not linear. In addition, 1 kHz may not be the most sensitive frequency to detect changes to the array produced by aging. The next step is to use this platform to compare how the simulated degradation of neural implants *in vitro* with the degradation of implants observed in *in vivo* experiments.

Supplementary Material

Refer to Web version on PubMed Central for supplementary material.

Acknowledgments

Authors would like to thank Dr Eugene Civillico, Dr Dinesh V Patwardhan and Dr Benita J Dair for their help with the project; Dr Katherine Vorvolakos and Dr Eric Sussman for providing the feedback on the manuscript; Defense Advanced Research Projects Agency Microsystems Technology Office (DARPA, MTO) for funding through an Interagency Agreement with the US Food and Drug Administration (FDA-DARPA 224-10-6006).

The mention of commercial products, their sources, or their use in connection with material reported herein is not to be construed as either actual or implied endorsement of such products by the Department of Health and Human Services.

References

Ali SAM, Zhong S-P, Doherty PJ, Williams DF. Mechanisms of polymer degradation in implantable devices: I. Poly(caprolactone). Biomaterials. 1993; 14:648–56. [PubMed: 8399961]

Atkins, P., Paula, JD. Physical Chemistry. 9. London: Macmillan; 2009.

Badwey JA, Karnovsky ML. Active oxygen species and the functions of phagocytic leukocytes. Annu. Rev. Biochem. 1980; 49:695–726. [PubMed: 6250449]

Barrese JC, Rao N, Paroo K, Triebwasser C, Vargas-Irwin C, Franquemont L, Donoghue JP. Failure mode analysis of silicon-based intracortical microelectrode arrays in nonhuman primates. J. Neural Eng. 2013; 10:066014. [PubMed: 24216311]

Bartels J, Andreasen D, Ehirim P, Mao H, Seibert S, Wright EJ, Kennedy P. Neurotrophic electrode: method of assembly and implantation into human motor speech cortex. J. Neurosci. Methods. 2008; 174:168–76. [PubMed: 18672003]

Bellamkonda R, Karumbaiah L, Saxena T, Wang Q, Stanley G. Is the extent of blood-brain-barrier breach predictive of intracortical electrode performance? Biophys. J. 2013; 104:376A–76A.

Biran R, Martin DC, Tresco PA. Neuronal cell loss accompanies the brain tissue response to chronically implanted silicon microelectrode arrays. Exp. Neurology. 2005; 195:115–26.

Branner A, Stein RB, Fernandez E, Aoyagi Y, Normann RA. Long-term stimulation and recording with a penetrating microelectrode array in cat sciatic nerve. IEEE Trans. Biomed. Eng. 2004; 51:146–57. [PubMed: 14723504]

Chestek CA, et al. Long-term stability of neural prosthetic control signals from silicon cortical arrays in rhesus macaque motor cortex. J. Neural Eng. 2011; 8:045005. [PubMed: 21775782]

Chichili GR, Nohr D, Frank J, Flaccus A, Fraser PD, Enfissi EMA, Biesalski HK. Protective effects of tomato extract with elevated beta-carotene levels on oxidative stress in ARPE-19 cells. Brit. J. Nutr. 2006; 96:643–9. [PubMed: 17010222]

Collinger JL, Wodlinger B, Downey JE, Wang W, Tyler-Kabara EC, Weber DJ, McMorland AJ, Velliste M, Boninger ML, Schwartz AB. High-performance neuroprosthetic control by an individual with tetraplegia. Lancet. 2013; 381:557–64. [PubMed: 23253623]

Davis EM, Benetatos NM, Regnault WF, Winey KI, Elabd YA. The influence of thermal history on structure and water transport in parylene C coatings. Polymer. 2011; 52:5378–86.

Dhillon GS, Horch KW. Direct neural sensory feedback and control of a prosthetic arm. IEEE Trans. Neural Syst. Rehabil. Eng. 2005; 13:468–72. [PubMed: 16425828]

Eisenberg G. Colorimetric determination of hydrogen peroxide. Ind. Eng. Chem. Anal. Ed. 1943; 15:327–8.

Freinbichler W, et al. Highly reactive oxygen species: detection, formation, and possible functions. Cell. Mol. Life Sci. 2011; 68:2067–79. [PubMed: 21533983]

Fries, RC. Reliable Design of Medical Devices. 3. Boca Raton, FL: CRC; 2012.

Gilgunn, PJ., Khilwani, R., Kozai, TDY., Weber, DJ., Cui, XT., Erdos, G., Ozdoganlar, OB., Fedder, GK. An ultra-compliant, scalable neural probe with molded biodissolvable delivery vehicle; 2012 IEEE 25th Int. Conf. on Micro Electro Mechanical Systems (MEMS); 2012. p. 56-9.

Giorgio M, Trinei M, Migliaccio E, Pelicci PG. Hydrogen peroxide: a metabolic by-product or a common mediator of ageing signals? Nat. Rev. Mol. Cell Biol. 2007; 8:722–8. [PubMed: 17700625]

Grill WM, Mortimer JT. Electrical properties of implant encapsulation tissue. Ann. Biomed. Eng. 1994; 22:23–33. [PubMed: 8060024]

Groothuis J, Ramsey NF, Ramakers GMJ, van der Plasse G. Physiological challenges for intracortical electrodes. Brain Stimulation. 2014; 7:1–6. [PubMed: 23941984]

Halliwell B. Reactive oxygen species and the central-nervous-system. J. Neurochem. 1992; 59:1609–23. [PubMed: 1402908]

Hochberg LR, Serruya MD, Friehs GM, Mukand JA, Saleh M, Caplan AH, Branner A, Chen D, Penn RD, Donoghue JP. Neuronal ensemble control of prosthetic devices by a human with tetraplegia. Nature. 2006; 442:164–71. [PubMed: 16838014]

Hochberg LR, et al. Reach and grasp by people with tetraplegia using a neurally controlled robotic arm. Nature. 2012; 485:372–U121. [PubMed: 22596161]

Hukins DWL, Mahomed A, Kukureka SN. Accelerated aging for testing polymeric biomaterials and medical devices. Med. Eng. Phys. 2008; 30:1270–4. [PubMed: 18692425]

Humphrey, DR., Schmidt, EM. Extracellular single-unit recording methods. In: Boulton, AA., et al., editors. Neurophysiological Techniques. New York: Humana; 1990. p. 1-64.

Judy JW. Neural interfaces for upper-limb prosthesis control: opportunities to improve long-term reliability. IEEE Pulse. 2012; 3:57–60.

Karumbaiah L, Saxena T, Carlson D, Patil K, Patkar R, Gaupp EA, Betancur M, Stanley GB, Carin L, Bellamkonda RV. Relationship between intracortical electrode design and chronic recording function. Biomaterials. 2013; 34:8061–74. [PubMed: 23891081]

Kim S-P, Simeral JD, Hochberg LR, Donoghue JP, Black MJ. Neural control of computer cursor velocity by decoding motor cortical spiking activity in humans with tetraplegia. J. Neural Eng. 2008; 5:455. [PubMed: 19015583]

Kozai TDY, Langhals NB, Patel PR, Deng X, Zhang H, Smith KL, Lahann J, Kotov NA, Kipke DR. Ultrasmall implantable composite microelectrodes with bioactive surfaces for chronic neural interfaces. Nat. Mater. 2012; 11:1065–73. [PubMed: 23142839]

Lempka SF, Miocinovic S, Johnson MD, Vitek JL, McIntyre CC. *In vivo* impedance spectroscopy of deep brain stimulation electrodes. J. Neural Eng. 2009; 6:046001. [PubMed: 19494421]

Lind G, Linsmeier CE, Schouenborg J. The density difference between tissue and neural probes is a key factor for glial scarring. Sci. Rep. 2013; 3:2942. [PubMed: 24127004]

Ludwig KA, Uram JD, Yang J, Martin DC, Kipke DR. Chronic neural recordings using silicon microelectrode arrays electrochemically deposited with a poly(3, 4-ethylenedioxythiophene) (PEDOT) film. J. Neural Eng. 2006; 3:59–70. [PubMed: 16510943]

Ludwig KA, Langhals NB, Joseph MD, Richardson-Burns SM, Hendricks JL, Kipke DR. Poly(3, 4-ethylenedioxythiophene) (PEDOT) polymer coatings facilitate smaller neural recording electrodes. J. Neural Eng. 2011; 8:014001. [PubMed: 21245527]

Malaga, K., Schroeder, KE., Patel, PR., Irwin, ZT., Thompson, DE., Chestek, CA., Patil, PG. Neuroscience Meeting Planner. Washington, DC: Society for Neuroscience; 2014. Data-driven model comparing the effects of glial scarring and interface interactions on chronic neural recordings. (online 638.12)

McConnell GC, Rees HD, Levey AI, Gutekunst C-A, Gross RE, Bellamkonda RV. Implanted neural electrodes cause chronic, local inflammation that is correlated with local neurodegeneration. J. Neural Eng. 2009; 6:056003. [PubMed: 19700815]

McGie SC, Nagai MK, Artinian-Shaheen T. Clinical ethical concerns in the implantation of brain-machine interfaces: II. Specific clinical and technical issues affecting ethical soundness. IEEE Pulse. 2013a; 4:32–7.

McGie SC, Nagai MK, Artinian-Shaheen T. Clinical ethical concerns in the implantation of brain-machine interfaces: I. Overview, target populations, and alternatives. IEEE Pulse. 2013b; 4:28–32.

Meijs GF, McCarthy SJ, Rizzardo E, Chen YC, Chatelier RC, Brandwood A, Schindhelm K. Degradation of medical-grade polyurethane elastomers: the effect of hydrogen peroxide *in vitro*. J. Biomed. Mater. Res. 1993; 27:345–56. [PubMed: 8360204]

Mercanzini A, Colin P, Bensadoun J-C, Bertsch A, Renaud P. *In vivo* electrical impedance spectroscopy of tissue reaction to microelectrode arrays. IEEE Trans. Biomed. Eng. 2009; 56:1909–18. [PubMed: 19362904]

Michael D, Travis ER, Wightman RM. Peer reviewed: color images for fast-scan CV measurements in biological systems. Anal. Chem. 1998; 70:586A–92A.

Moffitt MA, McIntyre CC. Model-based analysis of cortical recording with silicon microelectrodes. Clin. Neurophysiol. 2005; 116:2240–50. [PubMed: 16055377]

Ohnishi K, Weir RF, Kuiken TA. Neural machine interfaces for controlling multifunctional powered upper-limb prostheses. Expert Rev. Med. Devices. 2007; 4:43–53. [PubMed: 17187470]

Patrick E, Orazem ME, Sanchez JC, Nishida T. Corrosion of tungsten microelectrodes used in neural recording applications. J. Neurosci. Methods. 2011; 198:158–71. [PubMed: 21470563]

Peuster M, Kaese V, Wuensch G, Wuebbolt P, Niemeyer M, Boekenkamp R, Fink C, Haferkamp H, Hausdorf G. Dissolution of tungsten coils leads to device failure after transcatheter embolisation of pathologic vessels. Heart. 2001; 85:703–4.

Polikov VS, Tresco PA, Reichert WM. Response of brain tissue to chronically implanted neural electrodes. J. Neurosci. Methods. 2005; 148:1–18. [PubMed: 16198003]

Prasad A, Sanchez JC. Quantifying long-term microelectrode array functionality using chronic *in vivo* impedance testing. J. Neural Eng. 2012; 9:026028. [PubMed: 22442134]

Prasad A, Xue Q-S, Sankar V, Nishida T, Shaw G, Streit WJ, Sanchez JC. Comprehensive characterization and failure modes of tungsten microwire arrays in chronic neural implants. J. Neural Eng. 2012; 9:056015. [PubMed: 23010756]

Raspopovic S, et al. Restoring natural sensory feedback in real-time bidirectional hand prostheses. Sci Transl. Med. 2014; 6:222ra19–a222ra19.

Roitbak T, Syková E. Diffusion barriers evoked in the rat cortex by reactive astrogliosis. Glia. 1999; 28:40–8. [PubMed: 10498821]

Rousche PJ, Normann RA. Chronic recording capability of the utah intracortical electrode array in cat sensory cortex. J. Neurosci. Methods. 1998; 82:1–15. [PubMed: 10223510]

Ryu SI, Shenoy KV. Human cortical prostheses: lost in translation? Neurosurg. Focus. 2009; 27:E5.

Sanchez JC, Alba N, Nishida T, Batich C, Carney PR. Structural modifications in chronic microwire electrodes for cortical neuroprosthetics: a case study. IEEE Trans. Neural Syst. Rehabil. Eng. 2006; 14:217–21. [PubMed: 16792298]

Santhanam G, Ryu SI, Yu BM, Afshar A, Shenoy KV. A high-performance brain-computer interface. Nature. 2006; 442:195–8. [PubMed: 16838020]

Saxena T, Karumbaiah L, Gaupp EA, Patkar R, Patil K, Betancur M, Stanley GB, Bellamkonda RV. The impact of chronic blood-brain barrier breach on intracortical electrode function. Biomaterials. 2013; 34:4703–13. [PubMed: 23562053]

Schmidt EM, Bak MJ, McIntosh JS. Long-term chronic recording from cortical neurons. Exp. Neurology. 1976; 52:496–506.

Schmidt EM, McIntosh JS, Bak MJ. Long-term implants of parylene-C coated microelectrodes. Med. Biol. Eng. Comput. 1988; 26:96–101. [PubMed: 3199908]

Schneider CA, Rasband WS, Eliceiri KW. NIH image to imagej: 25 years of image analysis. Nat. Methods. 2012; 96:71–5.

Seymour JP, Kipke DR. Neural probe design for reduced tissue encapsulation in CNS. Biomaterials. 2007; 28:3594–607. [PubMed: 17517431]

Seymour JP, Elkasabi YM, Chen H-Y, Lahann J, Kipke DR. The insulation performance of reactive parylene films in implantable electronic devices. Biomaterials. 2009; 30:6158–67. [PubMed: 19703712]

Simeral JD, Kim S-P, Black MJ, Donoghue JP, Hochberg LR. Neural control of cursor trajectory and click by a human with tetraplegia 1000 days after implant of an intracortical microelectrode array. J. Neural Eng. 2011; 8:025027. [PubMed: 21436513]

Skousen JL, Merriam SME, Srivannavit O, Perlin G, Wise KD, Tresco PA. Reducing surface area while maintaining implant penetrating profile lowers the brain foreign body response to chronically implanted planar silicon microelectrode arrays. Prog. Brain Res. 2011; 194:167–80. [PubMed: 21867802]

Spataro L, Dilgen J, Retterer S, Spence AJ, Isaacson M, Turner JN, Shain W. Dexamethasone treatment reduces astroglia responses to inserted neuroprosthetic devices in rat neocortex. Exp. Neurology. 2005; 194:289–300.

Szarowski DH, Andersen MD, Retterer S, Spence AJ, Isaacson M, Craighead HG, Turner JN, Shain W. Brain responses to micro-machined silicon devices. Brain Res. 2003; 983:23–35. [PubMed: 12914963]

Thelin J, Jörntell H, Psouni E, Garwicz M, Schouenborg J, Danielsen N, Linsmeier CE. Implant size and fixation mode strongly influence tissue reactions in the CNS. PLoS ONE. 2011; 6:e16267. [PubMed: 21298109]

Tien LW, Wu F, Tang-Schomer MD, Yoon E, Omenetto FG, Kaplan DL. Silk as a multifunctional biomaterial substrate for reduced glial scarring around brain-penetrating electrodes. Adv. Funct. Mater. 2013; 23:3185–93.

Vetter RJ, Williams JC, Hetke JF, Nunamaker EA, Kipke DR. Chronic neural recording using silicon-substrate microelectrode arrays implanted in cerebral cortex. IEEE Trans. Biomed. Eng. 2004; 51:896–904. [PubMed: 15188856]

Ward MP, Rajdev P, Ellison C, Irazoqui PP. Toward a comparison of microelectrodes for acute and chronic recordings. Brain Res. 2009; 1282:183–200. [PubMed: 19486899]

Ware T, Simon D, Arreaga-Salas DE, Reeder J, Rennaker R, Keefer EW, Voit W. Fabrication of responsive, softening neural interfaces. Adv. Funct. Mater. 2012; 22:3470–9.

Welle C, Krauthamer V. FDA regulation of invasive neural recording electrodes: a daunting task for medical innovators. IEEE Pulse. 2012; 3:37–41. [PubMed: 22481744]

Williams JC, Hippensteel JA, Dilgen J, Shain W, Kipke DR. Complex impedance spectroscopy for monitoring tissue responses to inserted neural implants. J. Neural Eng. 2007; 4:410–23. [PubMed: 18057508]

Wolpaw, J., Wolpaw, EW. Brain-Computer Interfaces: Principles and Practice. Oxford: Oxford University; 2011.

Yokoyama K, Ogawa T, Fujita A, Asaoka K, Sakai J. Fracture of Ni–Ti superelastic alloy under sustained tensile load in physiological saline solution containing hydrogen peroxide. J. Biomed. Mater. Res. A. 2007; 82:558–67. [PubMed: 17311316]

Zhao Q, Casas-Bejar J, Urbanski P, Stokes K. Glass wool-H_2O_2/$CoCl_2$ test system for *in vitro* evaluation of biodegradative stress cracking in polyurethane elastomers. J. Biomed. Mater. Res. 1995; 29:467–75. [PubMed: 7622531]

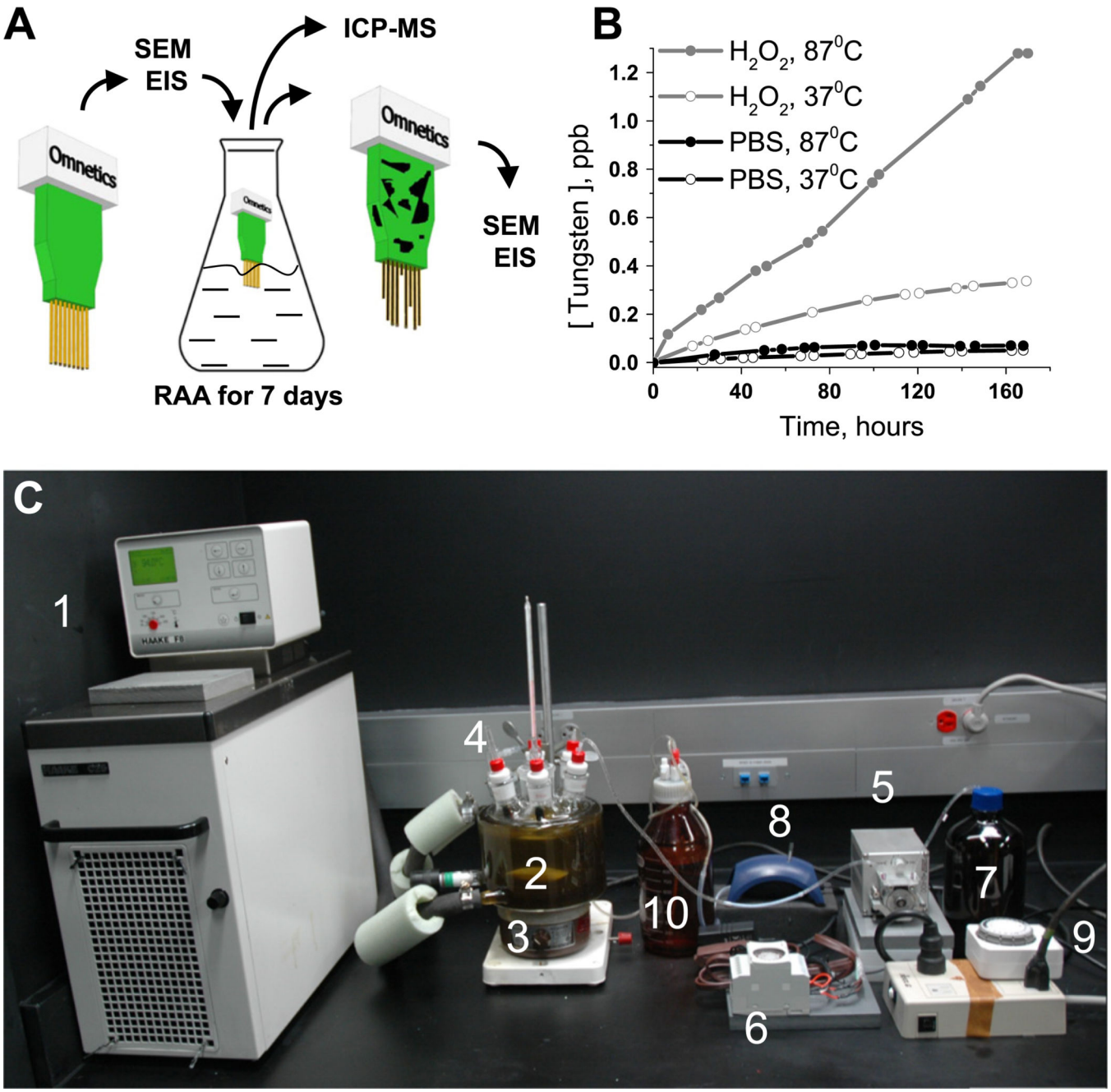

Figure 1.

Experimental setup for the reactive accelerated aging (RAA) of neural implants. Neural implants were characterized with scanning SEM and EIS before and after the RAA and the liquid from the reactor was analyzed with ICP-MS (A). ICP-MS data for concentration of tungsten in the reactor during RAA of TDT arrays for 7 days at four different conditions (at 37 °C and 87 °C with presence and absence of H_2O_2). The experimental system (C) was composed of: (1) thermostat; (2) flask with seven ports; (3) magnetic stirrer; (4) implant holders; (5) peristaltic pump for delivery of H_2O_2; (6) timer to control the peristaltic pump;

(7) bottle with concentrated H_2O_2; (8) vacuum drainage pump; (9) timer to control drainage pump; (10) waste bottle.

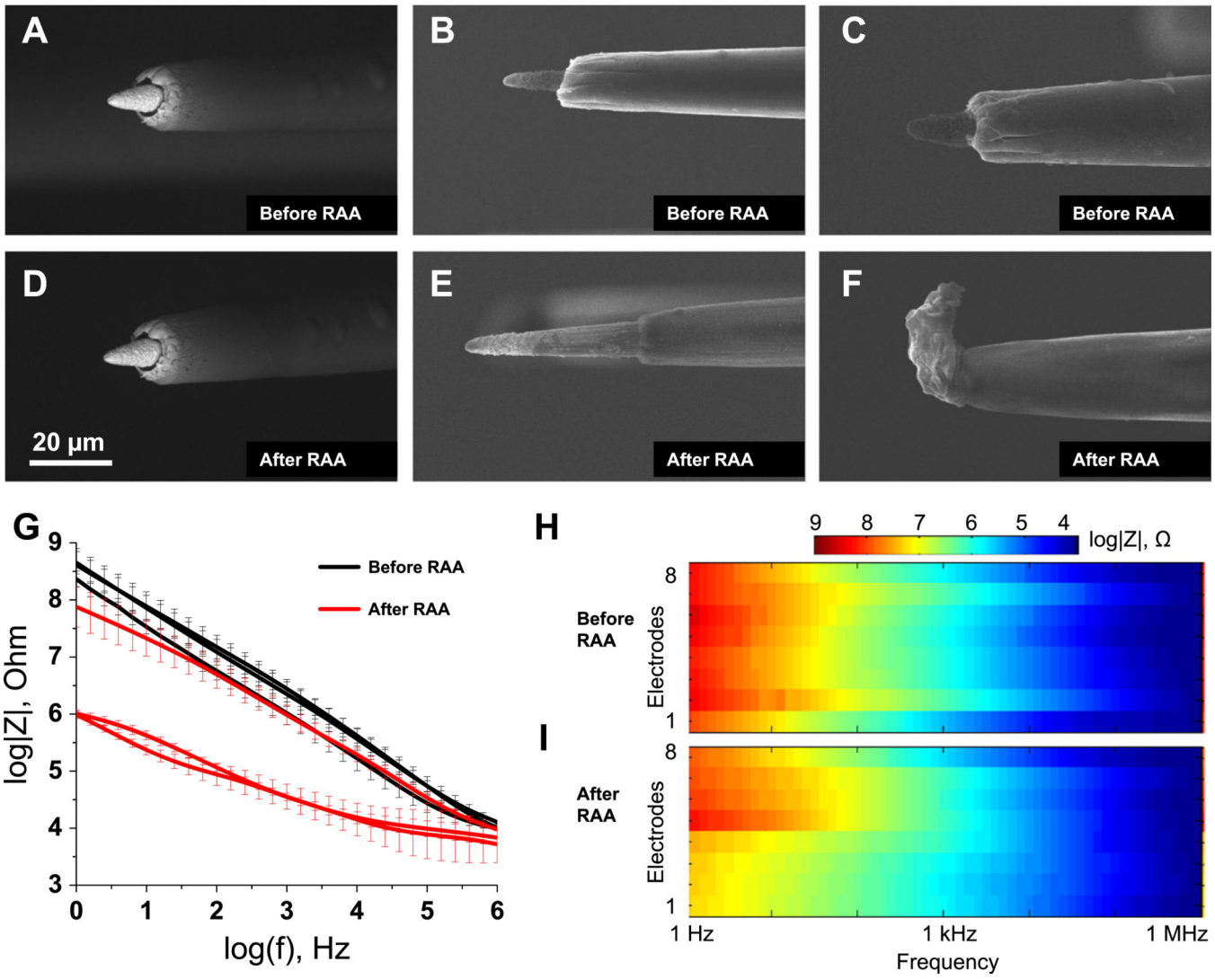

Figure 2.

Effect of the reactive accelerated aging (RAA) on the Microprobes neural implants examined with SEM and EIS. Electron micrographs of three representative electrodes before (A), (B) and (C) and after (D), (E) and (F) the RAA for 7 days at 87 °C in a solution of H_2O_2 in PBS. The impedance spectra for three implants before (black traces) and after (red traces) the RAA (G). The solid traces represent the mean for eight electrodes in each implant and the whiskers represent the relative standard deviation. Full impedance spectra presented as pseudocolor plots before (H) and after (I) the RAA for all eight microelectrodes of a representative implant with frequency located on the abscissa, electrode number located on the ordinate and color coding for the impedance magnitude.

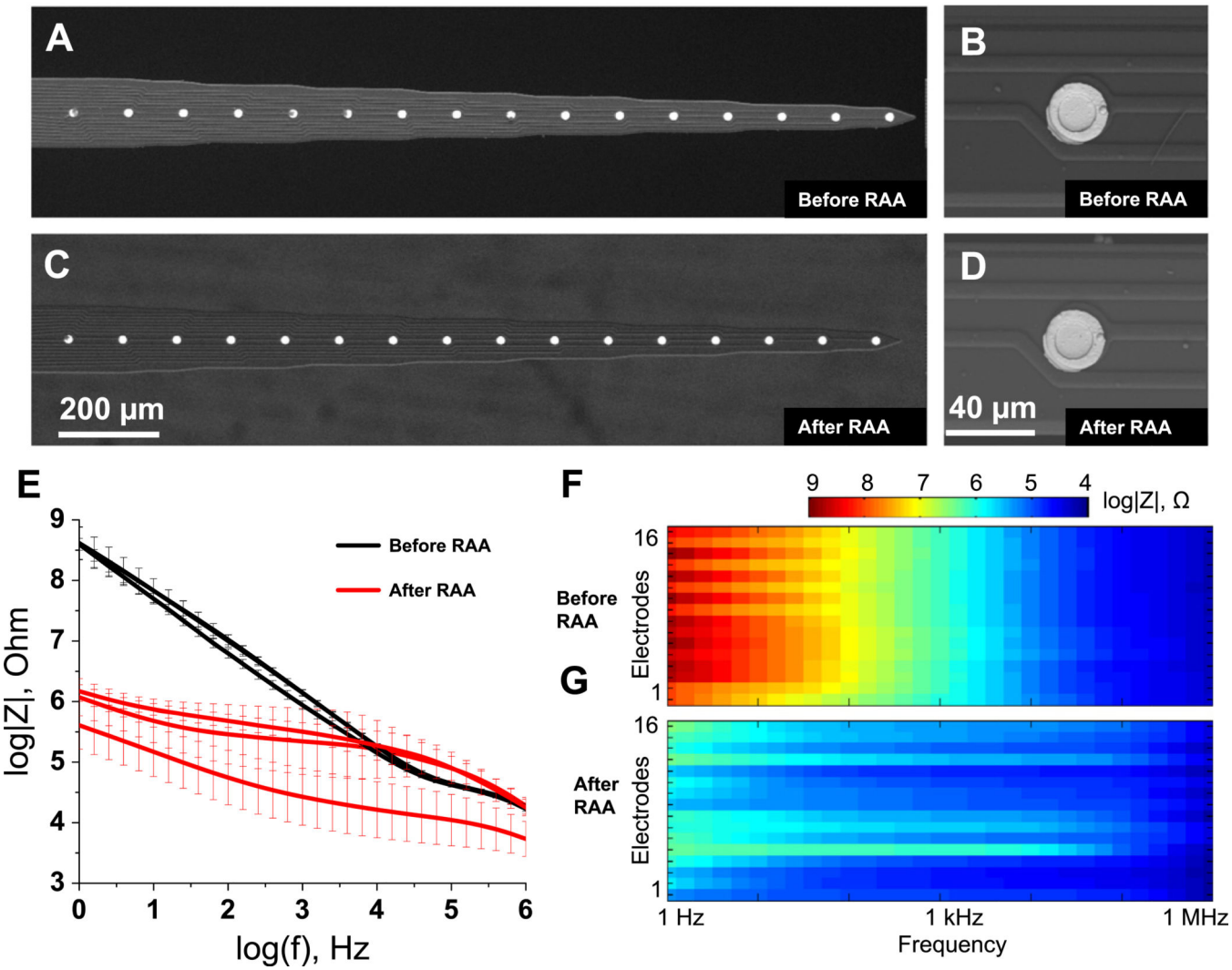

Figure 3.

Effect of the reactive accelerated aging (RAA) on the NeuroNexus neural implants examined with SEM and EIS. Electron micrographs of a representative neural implant before (A) and (C) and after (B) and (D) the RAA aging for 7 days at 87 °C in a solution of hydrogen peroxide in PBS. The impedance spectra for three implants before (black traces) and after (red traces) the RAA (E). The solid traces represent the mean for 16 electrodes in each implant and the whiskers represent the relative standard deviation. Full impedance spectra presented as pseudocolor plots before (F) and after (G) the RAA for all 16 microelectrodes of a representative implant with frequency located on the abscissa, electrode number located on the ordinate and color coding for the impedance magnitude.

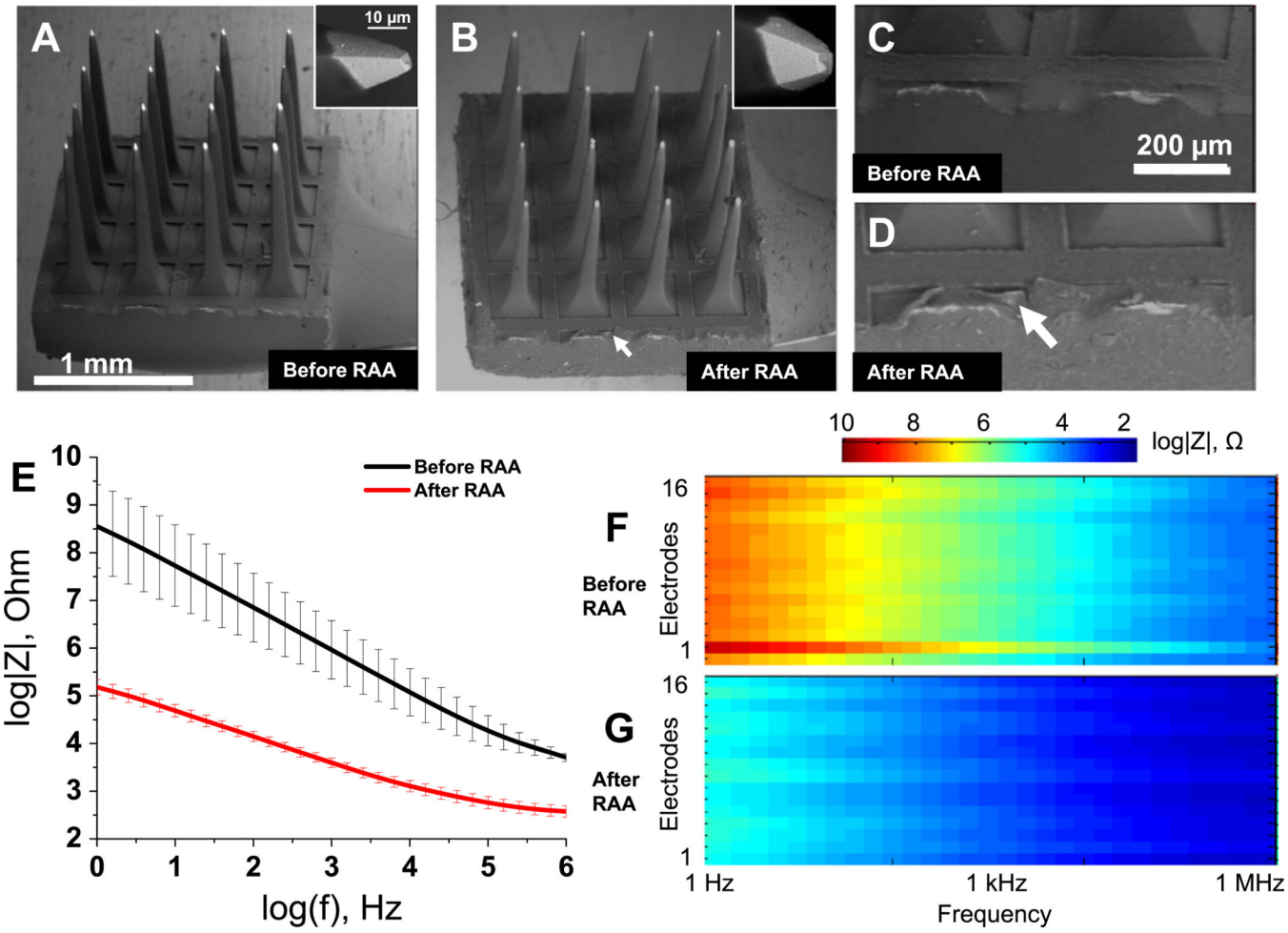

Figure 4.

Effect of the reactive accelerated aging (RAA) on the Blackrock neural implant examined with SEM and EIS. Electron micrographs of a neural implant before (A) and after (B) the RAA aging for 7 days at 87 °C in a solution of hydrogen peroxide in PBS. The neural implant frame at the higher magnification before (C) and after (D) the RAA with the white arrow pointing to delamination of insulation. The impedance spectra for an implant before (black traces) and after (red traces) the RAA (E). The solid traces represent the mean for 16 electrodes and the whiskers represent the relative standard deviation. Full impedance spectra presented as pseudocolor plots before (F) and after (G) the RAA for all 16 microelectrodes of an implant with frequency located on the abscissa, electrode number located on the ordinate and color coding for the impedance magnitude.

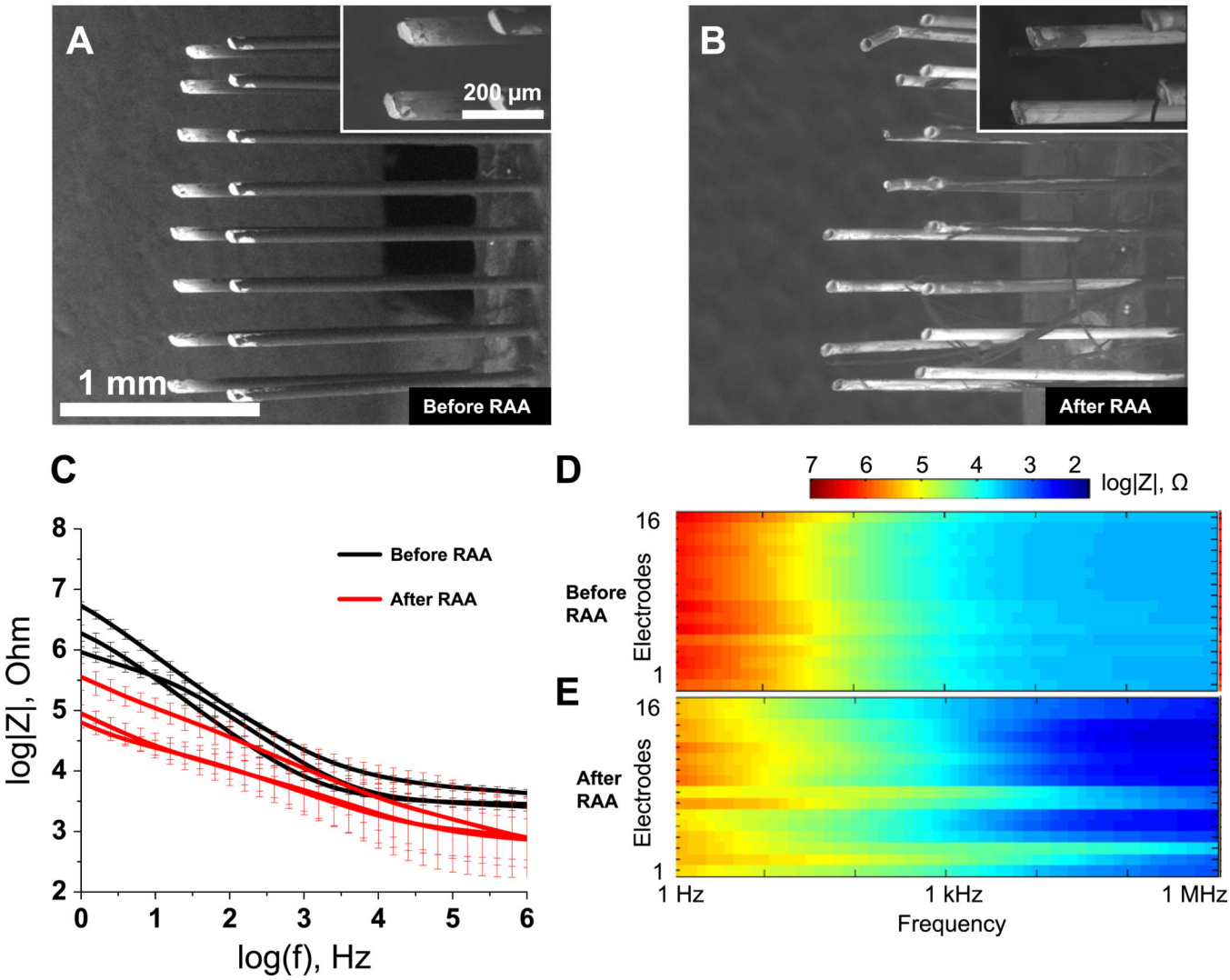

Figure 5.

Effect of the reactive accelerated aging (RAA) on the TDT neural implants examined with SEM and EIS. Electron micrographs of a representative neural implant before (A) and after (B) the RAA aging for 7 days at 87 °C in a solution of hydrogen peroxide in PBS. The impedance spectra for three implants before (black traces) and after (red traces) the RAA (C). The solid traces represent the mean for 16 electrodes in each implant and the whiskers represent the relative standard deviation. Full impedance spectra presented as pseudocolor plots before (D) and after (E) the RAA for all 16 microelectrodes of a representative implant with frequency located on the abscissa, electrode number located on the ordinate and color coding for the impedance magnitude.

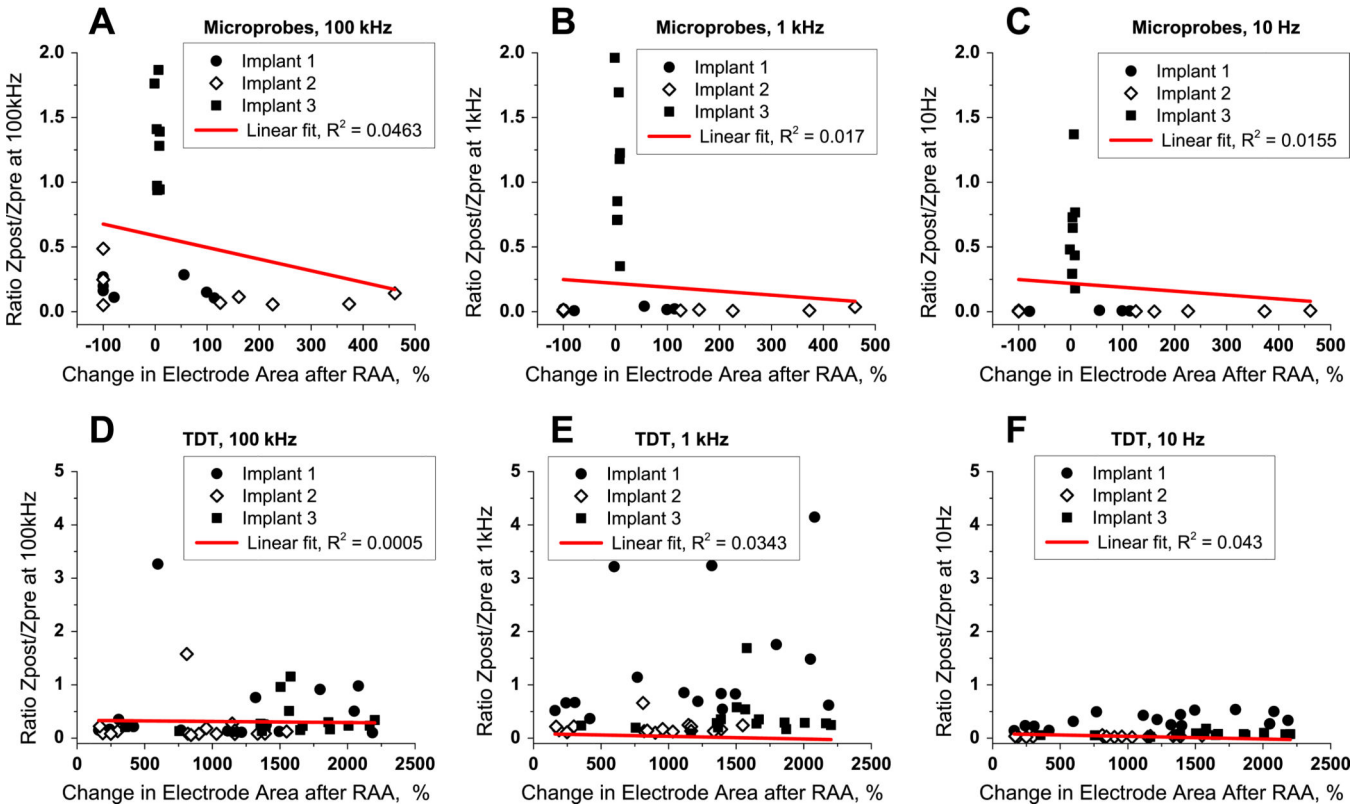

Figure 6.

Correlation between changes observed with microscopy and impedance spectroscopy for Microprobes and TDT neural implants after reactive accelerated aging (RAA). Ratio between impedance post-RAA and pre-RAA is plotted versus change in the exposed metal electrode for each electrode of Microprobe implants at frequencies 100 kHz (A), 1 kHz (B) and 10 Hz (C) and for each electrode of TDT implants at frequencies 100 kHz (D), 1 kHz (E) and 10 Hz (F). The filled circle, filled square and open diamond represents electrodes from each of the implants. Red line is a linear fit for all the electrodes from either Microprobes or TDT implants for each of the three frequencies with the correlation coefficients R^2 shown on the plots.

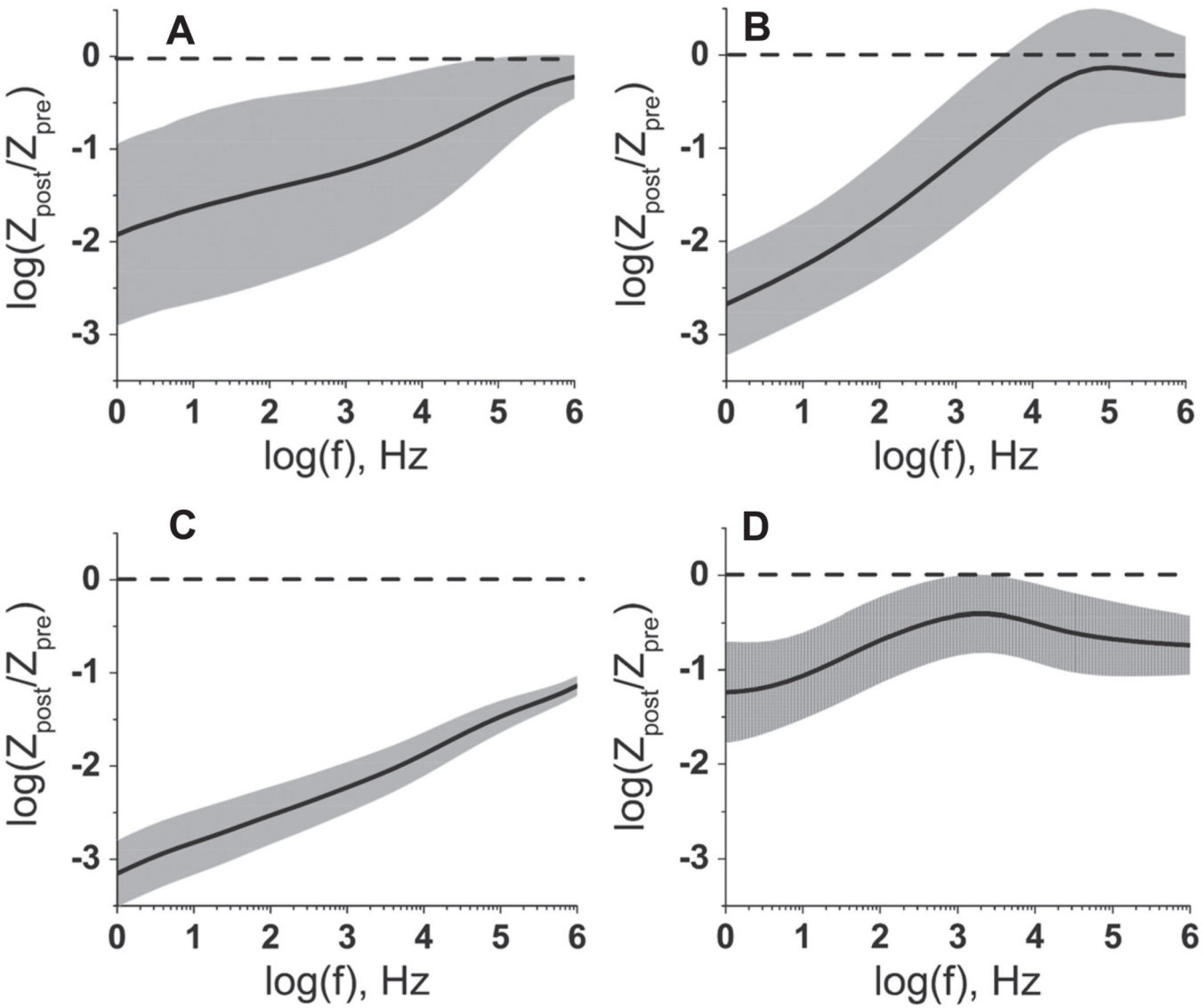

Figure 7.

Change in the impedance magnitude at different frequencies after the reactive accelerated aging (RAA). Change in the magnitude of impedance, at different frequencies after the RAA for Microprobes (A), NeuroNexus (B), Blackrock (C) and TDT (D) neural implants. The mean (solid black line) and the standard deviation (shaded gray area) of the relative change were calculated for 48 electrodes and 3 neural implants (NeuroNexus and TDT); 24 electrodes and 3 neural implants (Microprobes) or for 16 electrodes (Blackrock). The dashed line indicates zero which corresponds to no change in impedance.